Supporting information

High-Rate Intercalation without Nanostructuring in Metastable Nb_2O_5 Bronze Phases

Kent J. Griffith, Alexander C. Forse, John M. Griffin, Clare P. Grey

Department of Chemistry, University of Cambridge, Cambridge CB2 1EW, UK

E-mail: cpg27@cam.ac.uk

Additional Li NMR Fitting Details

To determine the nuclear quadrupolar coupling constant (C_Q) and quadrupolar asymmetry (η_Q), a global fit of the central peak and rotational sidebands was performed across spectra of ^{6}Li and ^{7}Li at 4.7 T and 16.4 T at 9kHz, 12.5 kHz, and 14 kHz MAS on each of the electrochemically lithiated samples at ambient temperature. Note that the ^{6}Li C_Q of a given environment is inherently reduced by a factor of 50 with respect to ^{7}Li and the simultaneous fitting of both isotopes is thus useful for parameter determination. Correlation times (τ_c) and activation energies (E_a) were derived from the variable temperature T_1 measurements at 4.7 T where the quadrupolar approximation is most relevant and dipolar or paramagnetic contributions are relatively minimal. Incorporating homonuclear dipolar coupling into a combined treatment of quadrupolar–dipolar relaxation lowers the theoretical T_1 minima but had no observable effect on the activation energies in this study. Furthermore, in the absence of any T_1 minima, the simplest model was chosen to analyze the data.

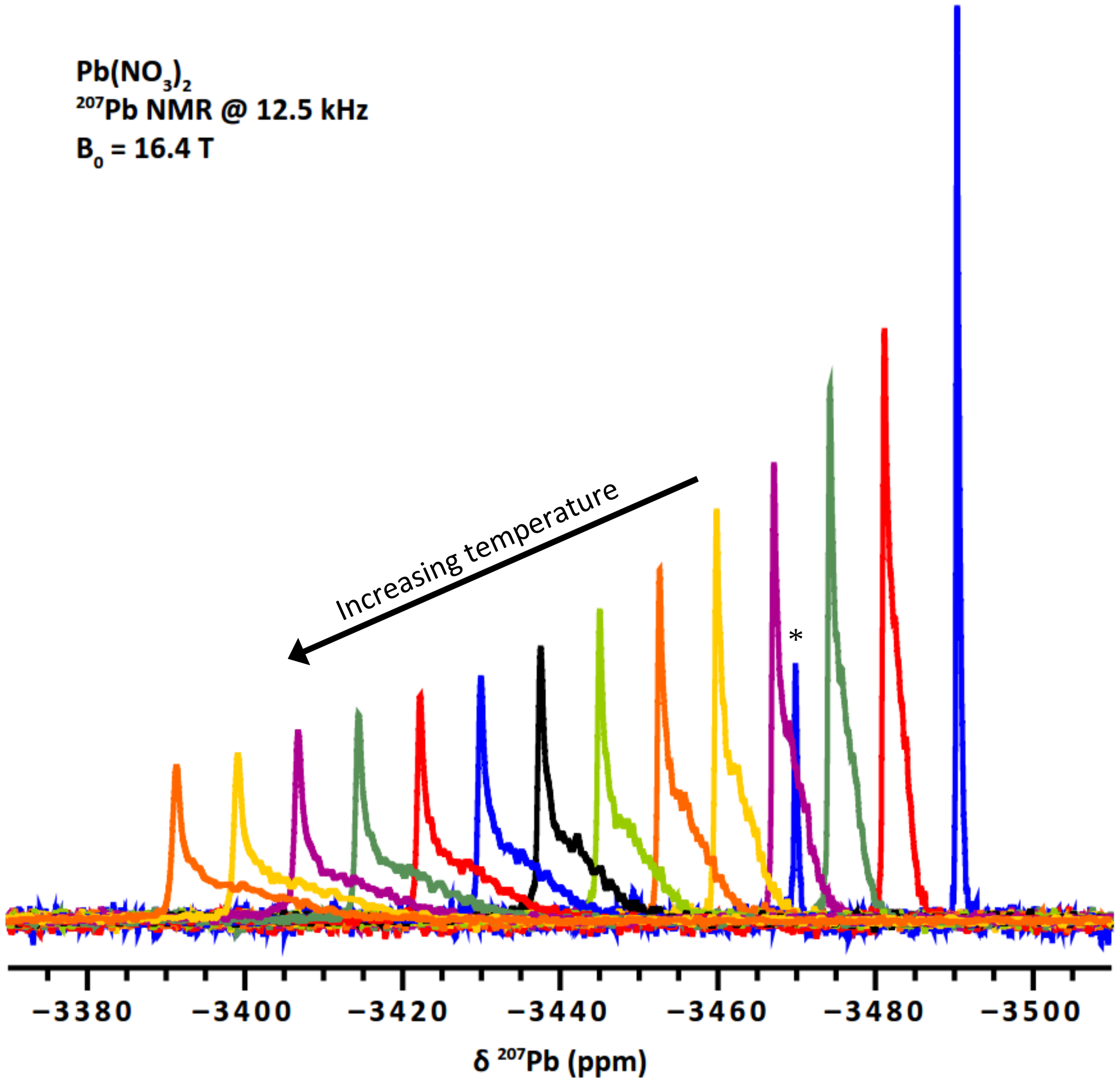

Supplementary Figure S1. ^{207}Pb Temperature Calibration on $Pb(NO_3)_2$ – As the zirconia rotor is heated, either from frictional heating or an external source, the ^{207}Pb chemical shift of lead nitrate shifts to the left (more positive frequency). There is a radial and longitudinal temperature gradient across a fully packed rotor, which is exacerbated as the temperature deviates from ambient conditions, giving rise to the increasing peak width at high temperature. All spectra were recorded under 12.5 kHz MAS conditions with the exception of the right-most spectra, which was spinning at 3 kHz MAS to minimize frictional heating. An asterisk denotes the rotational sideband from the sample at 3 kHz MAS. The temperature range 298 K to 424.8 K is depicted. In the absence of external heating, the rotor is heated to *ca*. 306 K at 12.5 kHz MAS via friction.

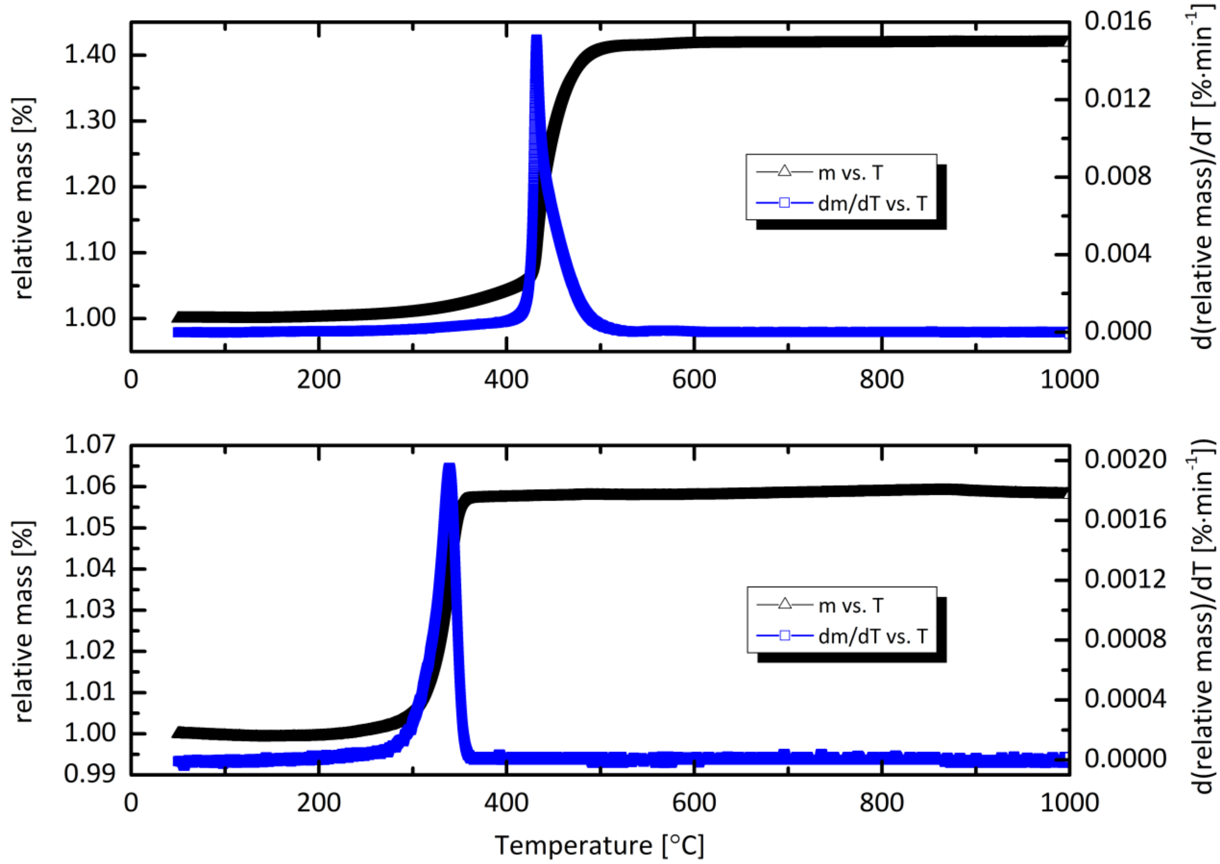

Supporting Figure S2. Mass and differential mass versus temperature curves of NbO_2 (lower) and Nb metal (upper) powders obtained under flowing air in a TGA.

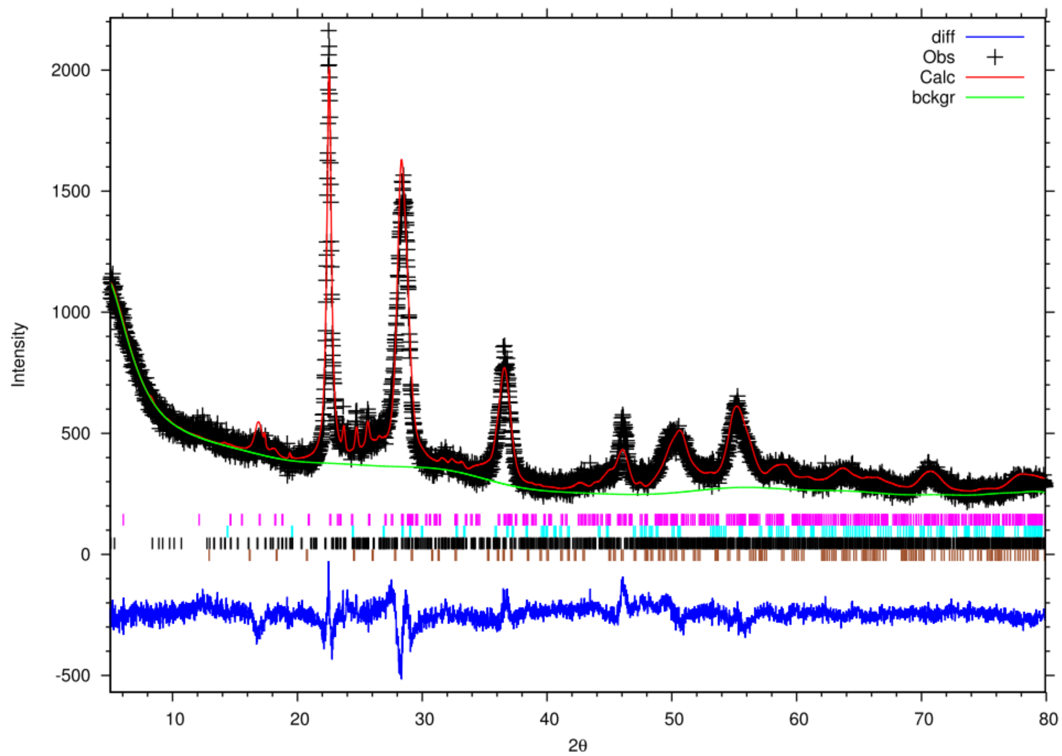

Supporting Figure S3a. Rietveld refinement of NbO_2 calcined at 300 °C for 24 h. Black crosses are observed data, solid red line is the calculated fit, lower solid blue line is the difference curve. Tick marks indicate expected {hkl} reflections for T-Nb_2O_5 (pink), B-Nb_2O_5 (light blue), H-Nb_2O_5 (black), and NbO_2 (brown). Structural data for the TT-phase are unavailable so a fit to the T-phase was performed. Phase analysis determined 91% (T)T-Nb_2O_5, 3% NbO_2, 3% B-Nb_2O_5, and 3% H-Nb_2O_5. Powder R factors: R_p = 0.0626, wR_p = 0.0806. Reduced χ^2 = 2.644.

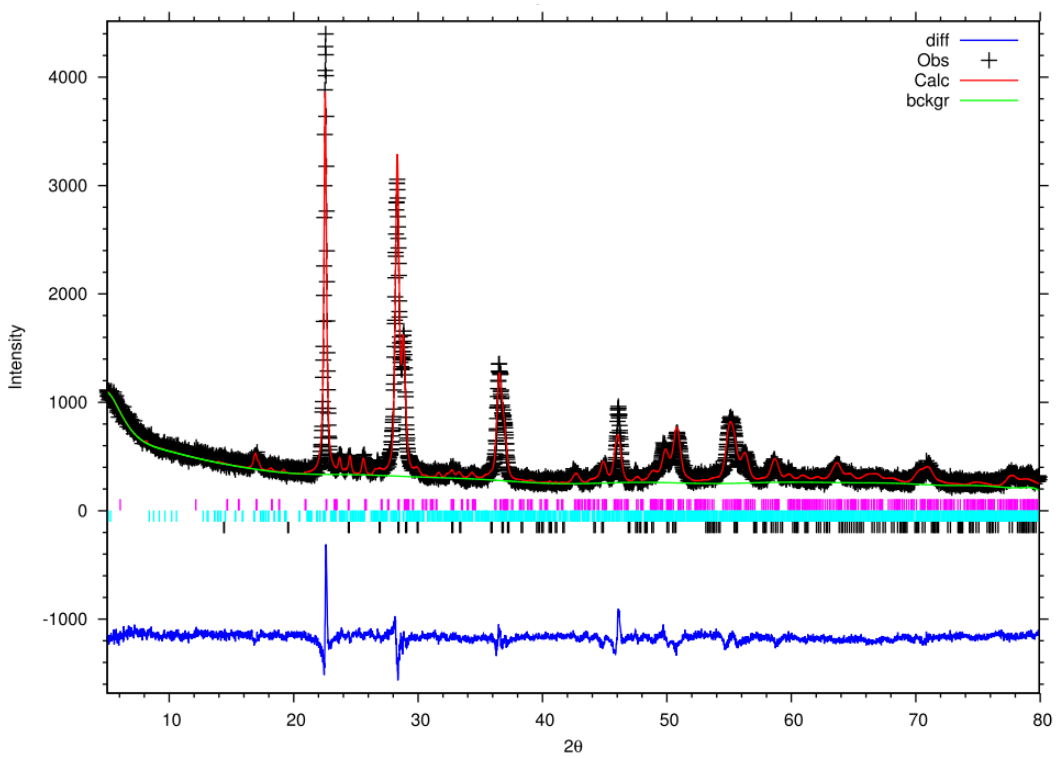

Supporting Figure S3b. Rietveld refinement of NbO_2 calcined at 600 °C for 24 h. Black crosses are observed data, solid red line is the calculated fit, lower solid blue line is the difference curve. Tick marks indicate expected {hkl} reflections for T-Nb_2O_5 (pink), H-Nb_2O_5 (light blue), and B-Nb_2O_5 (black). Phase analysis determined 92% T-Nb_2O_5, 5% B-Nb_2O_5, and 3% H-Nb_2O_5. Powder R factors: R_p = 0.0677, wR_p = 0.0867. Reduced χ^2 = 3.232.

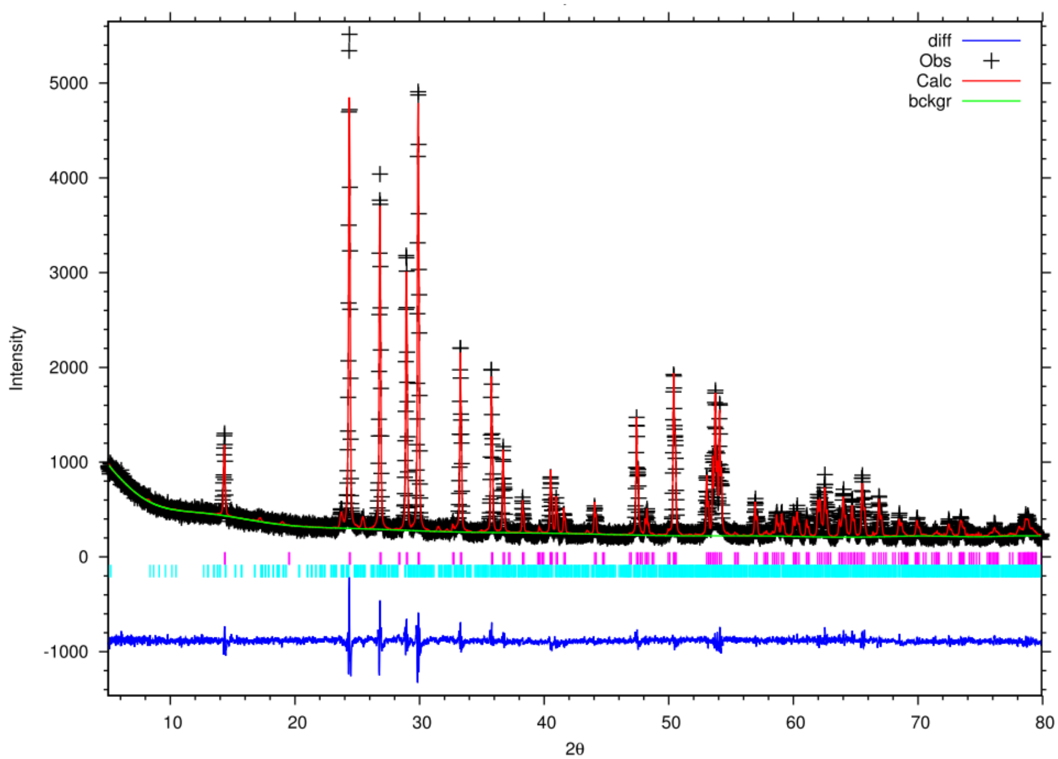

Supporting Figure S3c. Rietveld refinement of NbO_2 calcined at 850 °C for 24 h. Black crosses are observed data, solid red line is the calculated fit, lower solid blue line is the difference curve. Tick marks indicate expected {hkl} reflections for B-Nb_2O_5 (pink) and H-Nb_2O_5 (light blue). Phase analysis determined 98% B-Nb_2O_5 and 2% H-Nb_2O_5. Powder R factors: $R_p = 0.0578$, $wR_p = 0.0754$. Reduced $\chi^2 = 2.226$.

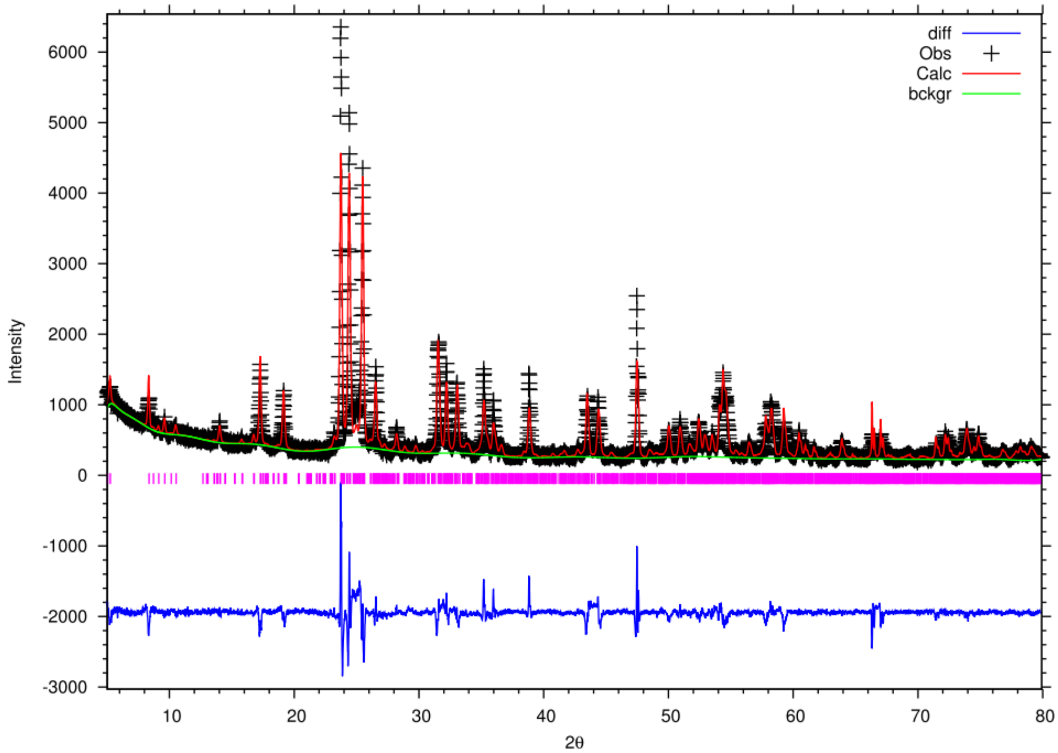

Supporting Figure S3d. Rietveld refinement of NbO_2 calcined at 1100 °C for 24 h. Black crosses are observed data, solid red line is the calculated fit, lower solid blue line is the difference curve. Tick marks indicate expected {hkl} reflections for H-Nb_2O_5 (pink). Phase analysis determined 100% H-Nb_2O_5. Powder R factors: R_p = 0.0875, wR_p = 0.1275. Reduced χ^2 = 7.803. The relatively poor fit of H-Nb_2O_5 may be related to the fact that the space group is H-Nb_2O_5 could be *P*2 rather than *P*2/*m*. A recent high-resolution neutron powder diffraction study[1] reported an improved fit in *P*2 but the single crystal *P*2/*m* was retained in this work as further elucidation of subtle crystallographic details is beyond the scope of the lab x-ray diffraction data collected for phase identification in this study.

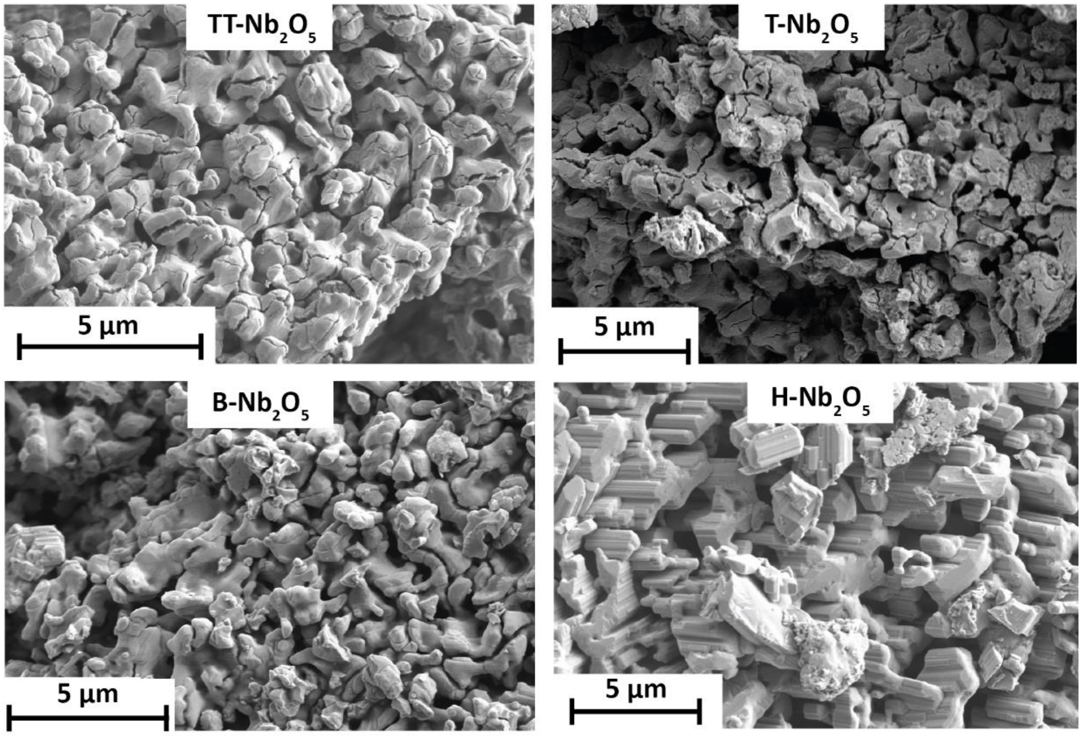

Supporting Figure S4. SEM image of TT-, T-, B-, and H-Nb_2O_5 showing the size and morphology of the agglomerated secondary particles (~20 µm) and their component primary domains (~1 µm). Each sub-figure contains one secondary particle; some secondary particle edges are visible (e.g. T-Nb_2O_5).

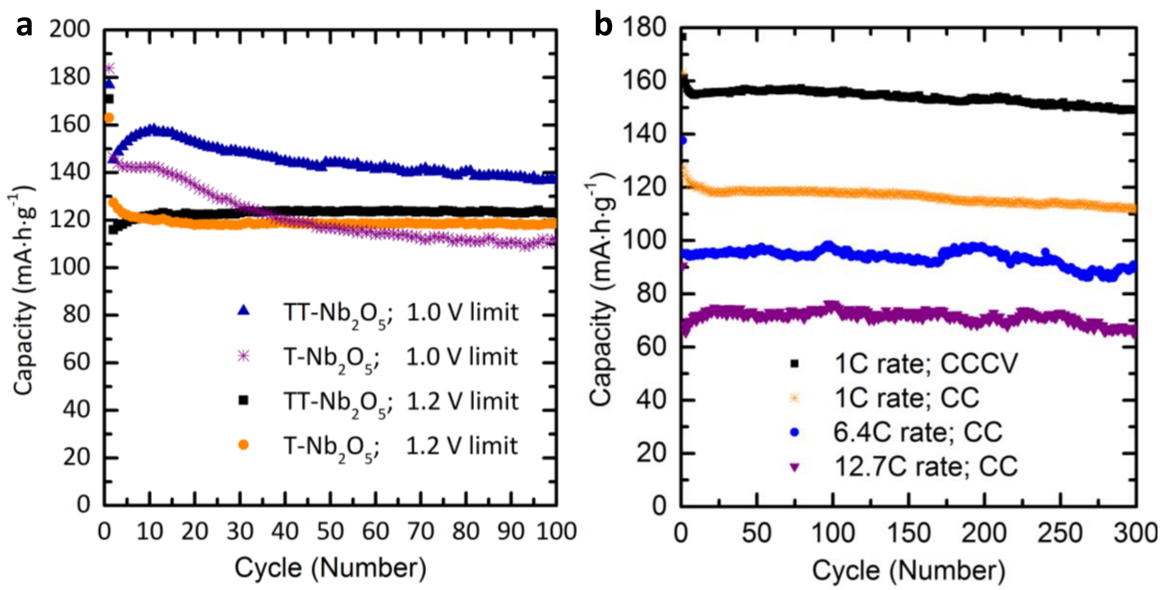

Supporting Figure S5. (a) At 1C, both T- and TT-Nb_2O_5 stably (de)intercalated 120 mA·h·g^{-1} from 3.0–1.2 V, 25% lower than under CCCV charging conditions. At the same rate but with a larger electrochemical window of 3.0–1.0 V, both phases showed a higher but less stable capacity. An increase in the capacity of TT-Nb_2O_5 over the first ten cycles was observed in all tests at both potential windows. (b) The capacity of T-Nb_2O_5 was stable over 300 cycles under various cycling conditions and, in all cases, the charge at a given current was the limiting step. The asymmetric charge–discharge behavior may be electronic and/or ionic in nature and will be discussed in detail in a future work.

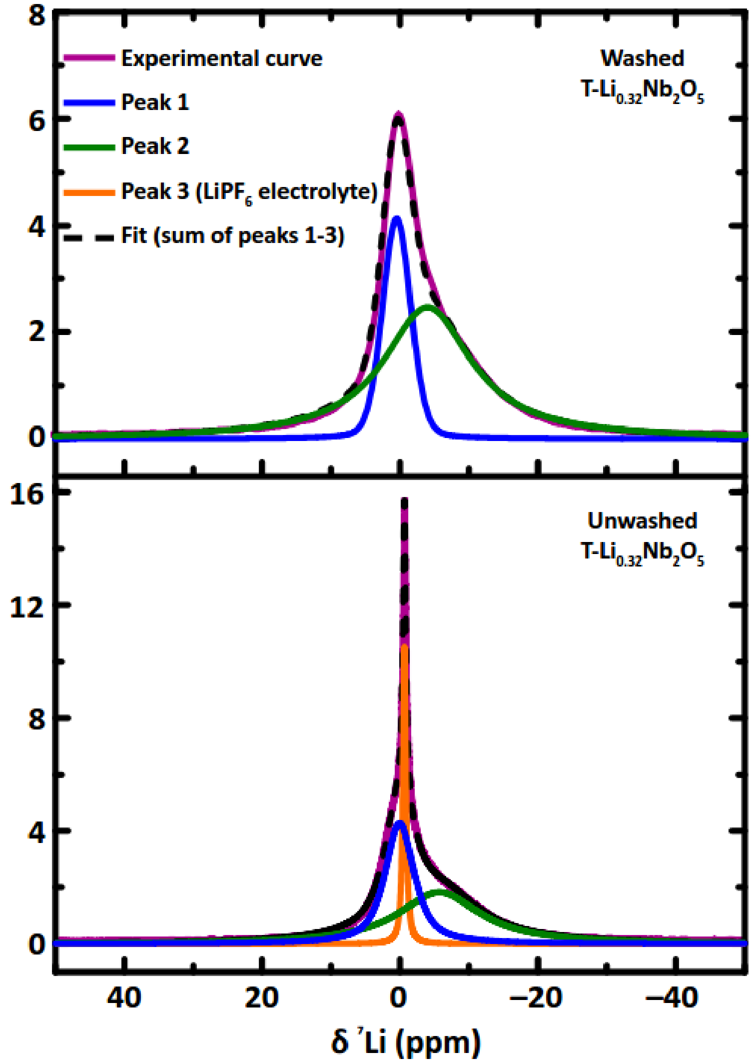

Supplementary Figure S6. ^{7}Li MAS NMR of T-$Li_{0.32}Nb_2O_5$ before and after washing in dimethyl carbonate. Spectra were recorded at 9 kHz MAS, 300 K, and magnetic field strength B_0 = 4.7 T. Central transition fitting parameters for both peaks from intercalated lithium (i.e. Peak 1 and Peak 2) were identical between the washed and unwashed sample. These results indicate i.) washing removes the LiPF6 peak entirely, ii.) washing has no effect on the intercalated lithium, and iii.) the intercalated lithium can be fit into two discrete NMR environments.

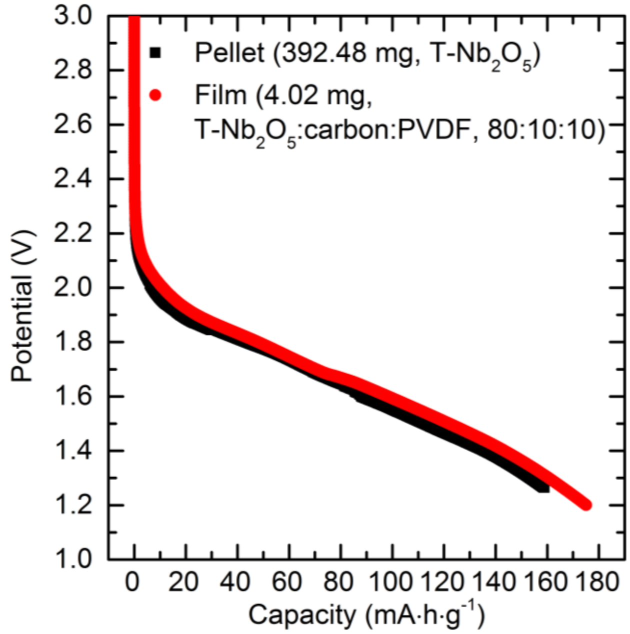

Supplementary Figure S7. Chronoamperometric comparison of lithiation into a *ca.* 150 µm thick film and a *ca.* 2.5 mm thick cold-pressed pellet of T-Nb_2O_5. The conventional film electrode was composed of T-Nb_2O_5:Super P carbon:PVDF in an 80:10:10 ratio as described in the main text while the pellet was pure T-Nb_2O_5 with no conductive additive or binder. Despite two orders of magnitude difference in active material mass and absence of carbon additive, the film and pellet electrodes showed similar electrochemical profiles. Note that the voltage cut-off was set to 1.20 V for the film and 1.25 V for the pellet.

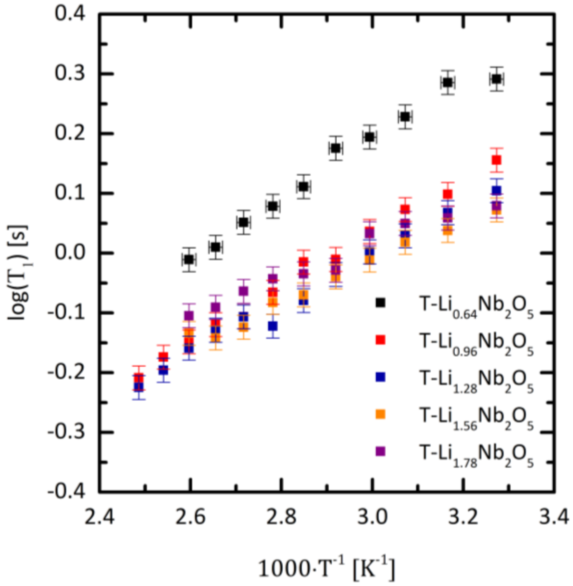

Supplementary Figure S8. The spin–lattice relaxation (T_1) for all samples and temperatures was on the order of $1x10^{-1}$ to $1x10^{1}$ seconds. On the low temperature flank of the T_1 minimum of the BPP model, T_1 decreases as temperature increases, as observed for all lithium concentrations in $Li_xNb_2O_5$ in this study.

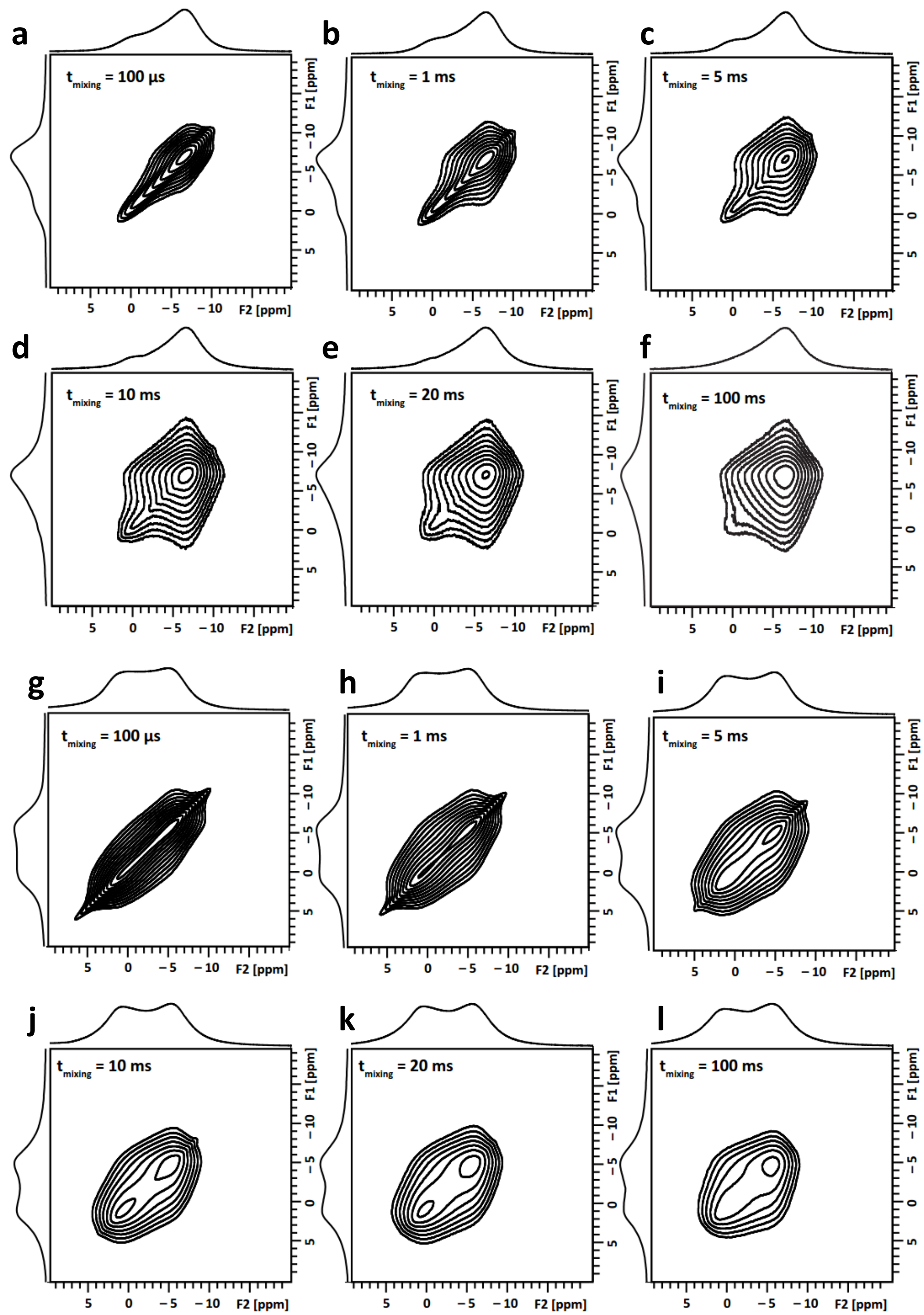

Supplementary Figure S9. ^{7}Li EXSY NMR spectra of T-$Li_{1.28}Nb_2O_5$ at 12.5 kHz MAS with mixing periods of (a) 100 µs (b) 1 ms (c) 5 ms (d) 10 ms (e) 20 ms and (f) 100 ms and T-$Li_{1.86}Nb_2O_5$ at 12.5 kHz MAS with mixing periods of (g) 100 µs (h) 1 ms (i) 5 ms (j) 10 ms (k) 20 ms and (l) 100 ms. The off-diagonal intensity at t_{mixing} = 100 µs is greater for further discharged samples (higher lithium content).

Supplementary References

1. Catti, M. & Ghaani, M. R. *Phys. Chem. Chem. Phys.* **2013**, *16*, 1385–1392.